Integrated control of vehicle stability by nonlinear observer-based exponential-like sliding mode neural network system

Hamid Taghavifar

Original citation & hyperlink:
Taghavifar, H., 2021. Integrated control of vehicle stability by nonlinear observer-based exponential-like sliding mode neural network system. *Proceedings of the Institution of Mechanical Engineers, Part D: Journal of Automobile Engineering* (In Press)
https://dx.doi.org/10.1177/09544070211014293

DOI 10.1177/09544070211014293
ISSN 0954-4070
ESSN 2041-2991

Publisher: Sage

Original Article

Institution of MECHANICAL ENGINEERS
Journal of AUTOMOBILE ENGINEERING

Proc IMechE Part D:
J Automobile Engineering
1–13

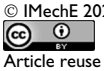

DOI: 10.1177/09544070211014293
journals.sagepub.com/home/pid
SAGE

Integrated control of vehicle stability by nonlinear observer-based exponential-like sliding mode neural network system

Hamid Taghavifar

Abstract

Dynamic stability is critical to achieve the safety of the cars, particularly during emergency maneuvers. Coordinated control algorithms are suggestive of the enhanced safety and stability of a vehicle. Hence, a novel adaptive robust multi-input control framework is developed using the combination of direct yaw moment (DYC) and active front steering (AFS). The dynamics of the steering system mechanism is included for the reliability of the proposed control scheme. The proposed controller is developed according to the approximation capacity of the radial basis function (RBF) neural network system. The adaptation laws are derived based on the Lyapunov stability theory. Additionally, the proposed integrated control paradigm contains a state observer and the sliding surface of the tracking errors converges to the asymptotic stability condition through the design of a smooth exponential reaching law. The effectiveness of the proposed control scheme is compared to a high-performance optimal robust control technique and open-loop system. In order to assess the robustness of the proposed algorithm, structured and unstructured uncertainties were also incorporated in terms of the parametric uncertainties such as the tire cornering stiffness and cross-wind gust disturbance. The results obtained for different maneuvers reveal that the proposed controller is successful to improve the handling performance and to ensure the stability of the vehicle when compared to the previously reported methods.

Keywords

Active front steering, direct yaw-moment control, exponential sliding surface, stability

Date received: 22 January 2021; accepted: 12 March 2021

Introduction

Vehicle motion control schemes have been massively evolved within the last couple of decades to respond to the demands on fuel efficiency, ride comfort, safety, and vehicle stability.[1,2] Invariants of control paradigms have been practiced concerning improved vehicle stability.[3,4] For instance, active front steering (AFS),[5,6] anti-lock braking systems (ABS),[7] and direct yaw-moment control (DYC)[8,9] are commonly regarded as effective methods to generate the required yaw stability and thus cornering performance. DYC is generally accomplished by producing an external yaw moment and using the differential braking system. For this purpose, an external yaw moment is applied to the chassis to improve vehicle active safety during aggressive driving maneuvers.[10] The optimal solution for the yaw moment and also the associated mechanism to generate the desired moment is still regarded as a challenge related to the implementation of the DYC approach.[11] Furthermore, the yaw moment is a bounded function of the road forces. Hence, the longitudinal tire forces can be typically insufficient to provide the necessary yaw moment particularly in case the vehicle inertia moment is also considerable.[12]

The control paradigms are designed and employed vastly in order to accomplish a certain performance as well as to meet vehicle security requirements.[13–15] Consequently, it is conceivable that distinct algorithms are bound to certain operating conditions. Therefore,

School of Mechanical, Aerospace and Automotive Engineering, Coventry University, Coventry, UK

Corresponding author:
Hamid Taghavifar, School of Mechanical, Aerospace and Automotive Engineering, Coventry University, Coventry CV15FB, UK.
Email: ad3380@coventry.ac.uk

the integrated control approaches such as AFS/DYC is a potentially effective means of enhanced vehicle lateral dynamics with no or a marginal interference between the different control parts of the coordinated system.[16–19] The integrated AFS/DYC has demonstrated conspicuous effectiveness to provide satisfactory performance for the vehicle in transient mode during critical maneuvers.[20] The vehicle handling control with uncertainties related to the vehicle parameters and states and subjected to external disturbances was explored employing a robust H_∞ dynamic feedback controller.[21] Furthermore, the effect of controller input saturation was investigated on the robustness of the proposed controller. Similarly, a robust fuzzy H_∞ control method was developed to improve the vehicle lateral stability and the handling dynamics by means of an integrated AFS + DYC algorithm wherein the nonlinear dynamics of the vehicle were modeled through a fuzzy system.[22] A hierarchical controller was developed based on an integrated AFS + DYC approach wherein the high-level controller was employed to generate a corrective yaw moment according to fast terminal sliding mode control in order to enhance the transient response of the system. The low-level counterpart was employed to convert the generated yaw into a corresponding longitudinal slip together with front steering input.[20]

The explored literature is suggestive that the integrated control frameworks related to the active chassis control systems uphold meritorious performance compared to their individual counterparts. However, further emerging control algorithms and novel control methods have yet to be involved to reach a well-established strategy.[16] The integrated control method has shown a higher performance in lane-change maneuvers and collision avoidance wherein the steering input demand has reduced by 20% when compared to the singularly front-axle steerable approach.[23] Consequently, it is comprehensible to further explore the capacity and the limits of the integrated control paradigm in light of the improved steerability and maneuverability as well as safety and stability during critical harsh maneuvers for automated cars and advanced driver-assistance systems. Apart from the control mechanism, the control algorithms which are explored above are suggestive of certain advantages but adaptive intelligent control techniques (e.g. Taghavifar[2], Taghavifar and Rakheja[5], and Mohammadzadeh and Taghavifar[6]) have demonstrated further effectiveness in terms of coping with systematic nonlinearities, providing rapid stabilization and significant robustness within a broad range of structured and unstructured uncertainties.

In light of the explored arguments, this paper proposes a novel control agenda to stabilize the vehicle lateral dynamics and provide motion stability and improved handling of vehicle by employing a coordinated DYC + AFS. It is aimed to follow the desired yaw rate and the sideslip angle of the vehicle obtained from a reference vehicle model. The developed algorithm is achieved by realizing the required yaw moment and front active steering input by employing a robust adaptive exponential-based integral sliding mode based RBF-NN (EISMC-RBF-NN) controller a sliding-mode controller wherein the system is subjected to parametric uncertainties and external disturbances and considering the region of nonlinearity and saturation of the tires with respect to the tire slip angle. The robustness of the proposed EISMC-RBF-NN control law is shown employing the Lyapunov stability theory. The effectiveness of the proposed controller is verified against a high-performance optimal robust control and without control systems in the literature,[13] by using co-simulation in CarSim and MATLAB/Simulink under various operating conditions. The main contributions of this study are described as:

- Unlike other papers, the nonlinear model dynamics for the observer and controller design is considered fully unknown.
- A novel exponential-like sliding surface with multi-rate convergence rate is proposed for removing the chattering drawback.
- The effectiveness of the proposed framework is tested during various emergency maneuvers and subject to strong gust of cross-wind validated using high-fidelity Matlab Simulink-Carsim co-simulations.

The remainder of the paper is organized as follows. In Section 2, the vehicle model is developed by incorporating a nonlinear tire model. The proposed control method is described in Section 3. In Section 4, the results are presented and discussed minutely. Finally, Section 5 summarizes the key findings of the paper and draws pertinent conclusions.

Problem statement

System modeling

Invariably speaking, pneumatic tires undertake the major task of generating directional forces to propel and to rotate the vehicle. Despite this, the lateral component of the tire force plays a substantial role in the handling stability and performance of the vehicle and the longitudinal forces influence the lateral dynamics infinitesimally. Although the kinematics and dynamics of the vehicle in the longitudinal orientation are dismissed, the vehicle speed must be sufficient to generate the lateral forces proportionally with the magnitude of slip angles according to the commonly employed tire models. Furthermore, no compliance is attributed in this study to the vehicle chassis as well as those of suspension systems while road is reasonably smooth and a geometric symmetricity exists between the left- and right-sides of the vehicle. Finally, it is assumed that the sway bar stiffness is large enough to resist weight transfer during the cornering maneuver. Under the above-described assumptions, a two-degree-of-freedom (2-

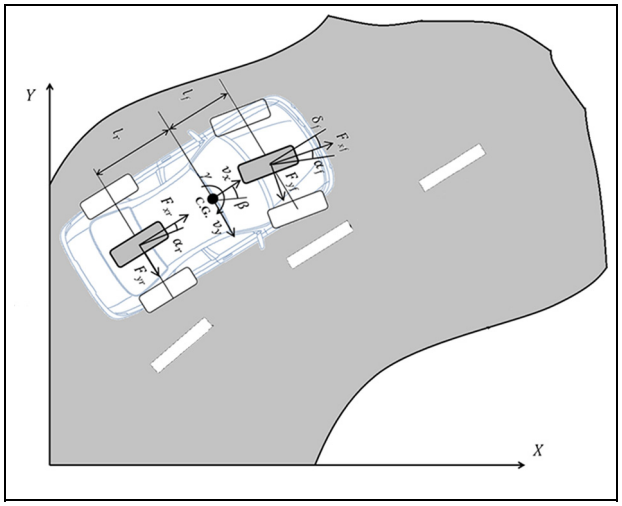

Figure 1. Yaw-plane 2-DoF model representation of the vehicle assuming right-and left-track symmetricity.

DOF) bicycle model is developed to describe the substantial handling dynamics modes of the vehicle (Figure 1).

Yaw stabilization is an imperative step toward improved handling performance which is usually accomplished through the convergence of vehicle yaw-rate γ to the desired yaw-rate. In order to derive the vehicle yaw rate γ it is sufficient to take the time derivative of heading angle φ. Additionally, the integrated AFS and DYC (AFS + DYC) strategy is suggestive of remarkable benefits among the various forms of the control strategies according to the reviewed literature.[22,24] In light of the arguments explored above, a 2-DOF yaw plane vehicle model is sufficiently capable to capture the main modes of motion for the vehicle lateral dynamics as follows:

$$\begin{aligned} \dot{v}_y &= \frac{1}{m}(F_{yf} + F_{yr}) - v_x\gamma \\ \dot{\gamma} &= \frac{1}{I_z}(F_{yf}\, l_f - F_{yr}\, l_r + \Delta T) \end{aligned} \tag{1}$$

where v_x and v_y denote the longitudinal and lateral speed components of the vehicle described in the body-attached reference system and $\dot{\varphi}$ and φ represent the vehicle yaw rate and heading angle terms, respectively. Furthermore, ΔT is the applied yaw moment, and F_{yf} and F_{yr} represent the tire lateral force components related to the front and rear wheels, respectively. Additionally, l_f and l_r are the front and rear wheelbase components, and m and I_z are the vehicle mass and yaw moment of inertia, respectively. The applied yaw moment to the vehicle with the track width l_b is characterized as:

$$\Delta T = \sum_i \sum_{j=1}^{2} (-1)^j F_{xij} \frac{l_b}{2} \tag{2}$$

where F_{xij} is the longitudinal force applied to the front and rear wheels. Based on the existing proportionality between the tire lateral force and the side slip angles, the lateral force components are definable in terms of the front and rear tire cornering stiffness (i.e. C_f and C_r):

$$F_{yf} = C_f\alpha_f, \quad F_{yr} = C_r\alpha_r \tag{3}$$

Additionally, the tire cornering stiffness saturation and nonlinearity is possible to be characterized in terms of the uncertainty around the nominal values:

$$C_f = \tilde{C}_f + \Delta C_f, \quad C_r = \tilde{C}_r + \Delta C_r \tag{4}$$

where $\widetilde{C}_f$ and $\widetilde{C}_r$ denote the nominal cornering stiffness parameters associated with the front and rear tires, respectively. Moreover, the nominal cornering stiffness components are representative of the tire force versus deflection in the linear region, and ΔC_f and ΔC_r account for the bounded uncertainties for tire cornering stiffness concerned with the front and rear wheels, respectively. Furthermore, the side slip angles related to the front and rear tires are simply stated as:

$$\begin{cases} \alpha_f = \arctan\left[\dfrac{v_x \sin(\beta) + l_f\gamma}{v_x \cos(\beta)}\right] - \delta_f \\ \alpha_r = \arctan\left[\dfrac{v_x \sin(\beta) - l_r\gamma}{v_x \cos(\beta)}\right] \end{cases} \tag{5}$$

Additionally, the steering system dynamics is also incorporated in the present study. According to the steering system dynamics (Figure 2), the tire lateral force produces a moment around the kingpin as follows:

$$T_s = 2(\sigma_c + \sigma_n)C_f\alpha_f \tag{6}$$

where σ_c and σ_n represent the castor and pneumatic trails, respectively. By replacing α_f from (5), (6) is rewritten as:

$$T_s = 2(\sigma_c + \sigma_n)C_f\left\{\arctan\left[\frac{v_x \sin(\beta) + l_f\gamma}{v_x \cos(\beta)}\right] - \delta_f\right\} \tag{7}$$

It is noteworthy that the moment is an external one applied to the front wheel and accordingly to the steering system. Therefore, the steering wheel governing equation of motion based on the rotation mode transferred about the kingpin is described as:

$$\begin{aligned} &I_s\left(\frac{d^2\delta}{dt^2} + \frac{d\gamma}{dt}\right) + C_s\frac{d\delta}{dt} - K_s(\vartheta - \delta) \\ &\quad = 2(\sigma_c + \sigma_n)C_f\left\{\arctan\left[\frac{v_x \sin(\beta) + l_f\gamma}{v_x \cos(\beta)}\right] - \delta_f\right\} \end{aligned} \tag{8}$$

It is noteworthy that the term $\dfrac{d\gamma}{dt}$ is added because the angular acceleration is relative to the absolute space and that the steering system being attached to the traveling vehicle. However, it is known that for the normal passenger cars $\dfrac{d^2\delta}{dt^2} \gg \dfrac{d\gamma}{dt}$. Hence, the developed steering system governing equation of motion is written as follows:

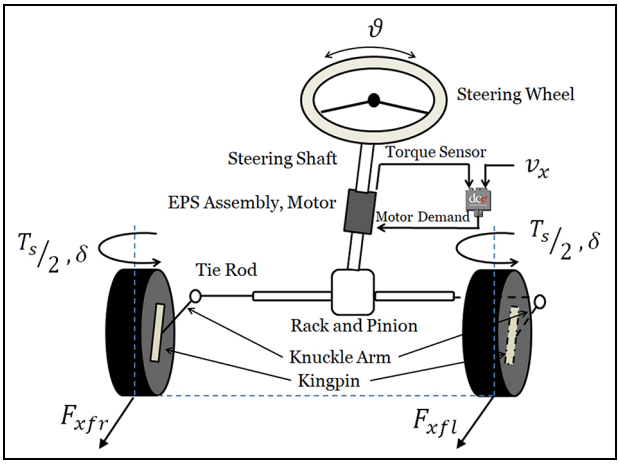

Figure 2. EPS-based steering system model considering steering-wheel torque feedback.

$$C_s\dot{\delta} = 2(\sigma_c + \sigma_n)C_f\left\{\arctan\left[\frac{v_x\sin\beta + l_f\gamma}{v_x\cos\beta}\right] - \delta\right\} + K_s(\vartheta - \delta) - I_s(\ddot{\delta}) \tag{9}$$

By rearranging the governing equations of motion for the vehicle lateral dynamics related to vehicle lateral speed, yaw-rate and steering system, and the steering system, the following is obtained:

$$\dot{v}_y = C_{f/m}\left\{\arctan\left[\frac{v_x\sin\beta + l_f\gamma}{v_x\cos\beta}\right] - \delta\right\} + C_{r/m}\left\{\arctan\left[\frac{v_x\sin\beta - l_r\gamma}{v_x\cos\beta}\right]\right\} - v_x\gamma \tag{10}$$

$$\dot{\gamma} = \left\{l_fC_{f/I_z}\left\{\arctan\left[\frac{v_x\sin\beta + l_f\gamma}{v_x\cos\beta}\right] - \delta\right\}\right\} + \left\{l_rC_{r/I_z}\left\{\arctan\left[\frac{v_x\sin\beta - l_r\gamma}{v_x\cos\beta}\right]\right\}\right\} + \Delta T/I_z \tag{11}$$

$$\dot{\delta} = 2(\sigma_c + \sigma_n)C_fC_s^{-1}\left\{\arctan\left[\frac{v_x\sin\beta + l_f\gamma}{v_x\cos\beta}\right] - \delta\right\} + K_sC_s^{-1}(\vartheta - \delta) \tag{12}$$

Accordingly, the general state-space representation of the system dynamics is derivable as follows:

$$\begin{cases} \dot{\underline{\xi}} = \underline{G}(\underline{\xi}) + \underline{H}(\underline{\xi})\underline{U} + \underline{d} \\ \underline{y} = C^T\underline{\xi} \end{cases} \tag{13}$$

where $\underline{\xi} = [v_y, \gamma, \delta]^T$ represents the states of the system, $\underline{G} = [g_1, g_2, g_3]^T$, denotes the nonlinear but bounded system function, $\underline{H} = diag(0, h_1, h_2)$ includes the general control function and $\underline{U} = [0, u_1, u_2]^T$ is the control input to the system, and $\underline{d}$ is vector of the bounded unknown external disturbance. Additionally, the corresponding subfunctions are obtained as:

$$g_1 = C_{f/m}\left\{\arctan\left[\frac{v_x\sin\beta + l_f\gamma}{v_x\cos\beta}\right] - \delta\right\} + C_{r/m}\left\{\arctan\left[\frac{v_x\sin\beta - l_r\gamma}{v_x\cos\beta}\right]\right\} - v_x\gamma \tag{14}$$

$$g_2 = \left\{l_fC_{f/I_z}\left\{\arctan\left[\frac{v_x\sin\beta + l_f\gamma}{v_x\cos\beta}\right] - \delta\right\}\right\} + \left\{l_rC_{r/I_z}\left\{\arctan\left[\frac{v_x\sin\beta - l_r\gamma}{v_x\cos\beta}\right]\right\}\right\} \tag{15}$$

$$g_3 = 2(\sigma_c + \sigma_n)C_fC_s^{-1}\left\{\arctan\left[\frac{v_x\sin\beta + l_f\gamma}{v_x\cos\beta}\right] - \delta\right\} - K_sC_s^{-1}\delta \tag{16}$$

Furthermore, it can be stated that $h_1 = 1/I_z$ and $h_2 = K_sC_s^{-1}$, $u_1 = \Delta T$ and $u_2 = \vartheta$. The reference signal $\underline{y}_d$ and tracking error vectors e are defined as follows:

$$\underline{e} = \underline{\xi} - \underline{y}_d \tag{17}$$

The desired yaw-rate and the body angle utilized as $\underline{y}_d$ are described in Aripin et al.[25] Therefore, one can rearrange (17) as follows:

$$\dot{\underline{\xi}} = \dot{-e} + \dot{\underline{y}}_d \tag{18}$$

Replacing (13) in (18) yields:

$$\dot{\underline{e}} + \dot{\underline{y}}_d = \underline{G}(\underline{\xi}) + \underline{H}(\underline{\xi})\underline{U} \tag{19}$$

By assuming $K_C = [k_{c1}, k_{c2}, k_{c3} \ldots, k_{cn}]^T$ as the gain vector is picked such that polynomial $s^n + k_{cn}s^{n-1} + \ldots + k_{c1}$ is Hurwitz stable.

$$\dot{\underline{e}} + K_C{}^T\underline{e} = 0 \tag{20}$$

Under the assumption that the system functions, $\underline{G}(\underline{\xi})$ and $\underline{H}(\underline{\xi})$, are known and the disturbance $\underline{d}(t)$ is zero, the linear feedback linearization offers that:

$$\bar{\underline{U}} = \underline{H}^{-1}(\underline{\xi})\left[-\underline{G}(\underline{\xi}) + \dot{\underline{y}}_d - K_C{}^T\underline{e}\right] \tag{21}$$

where $\bar{\underline{U}}$ represents the ideal control input on the above-described condition. Additionally, (21) can be further expanded to address the singularity problem by introducing the small positive constant ϕ, and bringing in D_c as the adaptive term incorporated to remove the influence of the approximation error and external disturbance in order to ensure the robustness of the closed-loop system.

$$\underline{U} = \left[\dot{\underline{y}}_d - \underline{G}(\underline{\xi}) - K_C{}^T\underline{e} + D_c\right]\left\{\underline{H}(\underline{\xi}) + \phi|\underline{H}(\underline{\xi})|\underline{H}^{-1}(\underline{\xi})\right\}^{-1} \tag{22}$$

However, the functions $\underline{G}(\underline{\xi})$ and $\underline{H}(\underline{\xi})$ as well as the system vector of states $\underline{\xi}$ are not always available. Thus, the estimated counterparts of these terms denoted by $\hat{\underline{G}}(\underline{\xi})$ and $\hat{\underline{H}}(\underline{\xi})$ are employed according to (24).

$$\underline{U} = \left[\dot{\underline{y}}_d - \hat{\underline{G}}\left(\hat{\underline{\xi}}\right) - {K_C}^T\hat{\underline{e}} + D_c\right] \left\{\hat{\underline{H}}\left(\hat{\underline{\xi}}\right) + \phi\left|\hat{\underline{H}}\left(\hat{\underline{\xi}}\right)\right|\hat{\underline{H}}^{-1}\left(\hat{\underline{\xi}}\right)\right\}^{-1} \tag{23}$$

By adding and subtracting the term $\{\hat{\underline{H}}(\hat{\underline{\xi}}) + \phi|\hat{\underline{H}}(\hat{\underline{\xi}})|\hat{\underline{H}}^{-1}(\hat{\underline{\xi}})\}$, (14) is rewritable as:

$$\begin{aligned}\dot{\underline{\xi}} &= \underline{G}(\underline{\xi}) + \left\{\underline{G}(\underline{\xi}) - \hat{\underline{H}}\left(\hat{\underline{\xi}}\right) - \left|\hat{\underline{H}}\left(\hat{\underline{\xi}}\right)\right|\hat{\underline{H}}^{-1}\left(\hat{\underline{\xi}}\right)\right\}\underline{U} \\ &+ \left\{\hat{\underline{H}}\left(\hat{\underline{\xi}}\right) + \left|\hat{\underline{H}}\left(\hat{\underline{\xi}}\right)\right|\hat{\underline{H}}^{-1}\left(\hat{\underline{\xi}}\right)\right\}\underline{U} + \underline{d} \\ \underline{y} &= C^T\underline{\xi}\end{aligned} \tag{24}$$

Based on the observed states and the reference signals, it is evident to obtain:

$$\dot{\underline{y}}_d = \underline{G}(\underline{y}_d) + \underline{H}(\underline{y}_d)\underline{U} \tag{25}$$

Additionally, by applying (23) to (24), one will get:

$$\begin{aligned}\dot{\underline{\xi}} = \underline{G}(\underline{\xi}) &+ \{\underline{H}(\underline{\xi}) - \hat{\underline{H}}(\hat{\underline{\xi}}) - |\hat{\underline{H}}(\hat{\underline{\xi}})|\hat{\underline{H}}^{-1}(\hat{\underline{\xi}})\}\underline{U} \\ &+ \dot{\underline{y}}_d - \hat{\underline{G}}(\hat{\underline{\xi}}) - \underline{K_C}^T\hat{\underline{e}} + \underline{D_c} + \underline{d}\end{aligned} \tag{26}$$

By plugging in (25) into (26), one will obtain the error dynamics as follows:

$$\begin{aligned}\dot{\underline{e}} = \underline{G}(\underline{e}) &+ \{\underline{H}(\underline{\xi}) - \hat{\underline{H}}(\hat{\underline{\xi}}) - |\hat{\underline{H}}(\hat{\underline{\xi}})|\hat{\underline{H}}^{-1}(\hat{\underline{\xi}})\}\underline{U} \\ &- \hat{\underline{G}}(\hat{\underline{\xi}}) - \underline{K_C}^T\hat{\underline{e}} + \underline{D_c} + \underline{d}\end{aligned} \tag{27}$$

Figure 3 represents the block diagram of the proposed control algorithm for improving the lateral stability of vehicles subject to external disturbances using the adaptive nonlinear state-observer and exponential sliding mode control scheme coupled to an optimization problem. In this paradigm, the NN observer estimates the unknown but limited functions of $\hat{\underline{G}}(\hat{\xi})$ and $\hat{\underline{H}}(\hat{\xi})$ and the adaptation rules are couple to the exponential sliding mode system. However, Chaos-PSO optimization defines the optimal design variables of the control scheme. The output controls are then transferred into the steering system in terms of the active front steering and direct yaw-moment. The final validation transpires through the co-simulation of MATLAB Simulink and Carsim software.

To conclude, the following assumptions are made from the vehicle dynamics point of view:

- A two-degree-of-freedom (2-DOF) bicycle model is sufficient to describe the fundamental handling characteristics.
- Road is smooth, no compliance for chassis and suspensions is attributed, and the traveling speed is constant during the critical maneuvers.
- The tire nonlinearity and saturation can be taken into account through the uncertainty functions from (4).

Neural networks

A neural network-based representation of the unknown functions $\underline{H}(\xi)$ and $\underline{G}(\xi)$ in an assumed compact set set $(\underline{H}(\xi)\ ,\ \underline{G}(\xi)\ \in \mathcal{R})$ is is presentable through estimation functions $W_{\underline{H}}^T\psi_H(\xi)$ and $V_{\underline{G}}^T\psi_{\underline{G}}(\xi)$, respectively, considering the entailed errors $\varepsilon(\underline{\xi}) = \left[\varepsilon_{\underline{H}}(\xi), \varepsilon_{\underline{G}}(\xi)\right]^T$ defined as[26]:

$$\begin{aligned}\underline{H}(\xi) &= W_{\underline{H}}^T\psi_H(\xi) + \varepsilon_{\underline{H}}(\xi) \\ \underline{G}(\xi) &= W_{\underline{G}}^T\psi_G(\xi) + \varepsilon_{\underline{G}}(\xi)\end{aligned} \tag{28}$$

where $W_{\underline{H}} = \left[W_{\underline{H}1}, W_{\underline{H}2}, \ldots, W_{\underline{H}n}\right]$ and $V_{\underline{G}} = \left[V_{\underline{G}1}, V_{\underline{G}2}, \ldots, V_{\underline{G}n}\right]$ characterize the vectors of NN for the associated functions and $\psi_{\underline{H}}(\xi) = [\psi_{\underline{H}1}(x), \psi_{\underline{H}2}(x), \ldots, \psi_{\underline{H}n}(x)]$ and $\psi_{\underline{G}}(\xi) = [\xi_{\underline{G}1}(x), \xi_{\underline{G}2}(x), \ldots, \xi_{\underline{G}n}(x)]$ are the vectors in the NN representation. Additionally, $\varepsilon_{\underline{H}}(\xi)$ and $\varepsilon_{\underline{G}}(\xi)$ are employed to perform the represent the errors of estimation errors for the developed system. The optimal estimation weights to accomplish the minimum errors are denotable as follows:

$$\begin{aligned}W_{\underline{H}}^* :&= \arg\min_{W_{\underline{H}}\in R}\left\{\sup_{\xi\in \mathrm{B}}\left|\underline{H}(\xi) - W_{\underline{H}}^T\varphi_{\underline{H}}(\xi)\right|\right\} \\ V_{\underline{G}}^* :&= \arg\min_{V_{\underline{G}}\in R}\left\{\sup_{\xi\in \mathrm{B}}\left|\underline{G}(\xi) - V_{\underline{G}}^T\varphi_{\underline{G}}(\xi)\right|\right\}\end{aligned} \tag{29}$$

The resulting arguments may be expanded according to the defined vectors of weight for NN and the associated optimal terms represented in (30):

$$\begin{aligned}\widehat{\underline{H}}(\xi|W_{\underline{H}}) - \widehat{\underline{H}}(\xi|W_{\underline{H}}^*) &= (W_{\underline{H}} - W_{\underline{H}}^*)^T\left[\frac{\partial\widehat{\underline{H}}(\xi|W_{\underline{H}})}{\partial W_{\underline{H}}}\right] \\ &+ h.o.t(|W_{\underline{H}} - W_{\underline{H}}^*|^2) \\ \widehat{\underline{G}}(\xi|V_{\underline{G}}) - \widehat{\underline{G}}(\xi|V_{\underline{G}}^*) &= (V_{\underline{G}} - V_{\underline{G}}^*)^T\left[\frac{\partial\widehat{\underline{G}}(\xi|V_{\underline{G}})}{\partial V_{\underline{G}}}\right] \\ &+ h.o.t(|W_{\underline{G}} - W_{\underline{G}}^*|^2)\end{aligned} \tag{30}$$

where the argument and $h.o.t(|W_{\underline{H}} - W_{\underline{H}}^*|^2)$ contains the higher order terms concerned with the estimations presented in (30). Moreover, the variable vectors in the approximation functions (30) are stated as:

$$\begin{aligned}\psi_{\underline{H}}(\xi|W_{\underline{H}}) &= \frac{\partial\widehat{\underline{H}}(\xi|W_{\underline{H}})}{\partial W_{\underline{H}}} \\ \psi_{\underline{G}}(\xi|V_{\underline{G}}) &= \frac{\partial\widehat{\underline{G}}(\xi|V_{\underline{G}})}{\partial V_{\underline{G}}}\end{aligned} \tag{31}$$

Therefore, once can represent the functions $\underline{H}(\xi, \dot{\xi}, \ldots, \xi^{(n-1)})$ and $\underline{G}(\xi, \dot{\xi}, \ldots, \xi^{(n-1)})$ related to the system dynamics expressed in (14) with $\varepsilon(x)$ in the form of the approximation error. Additionally, it is

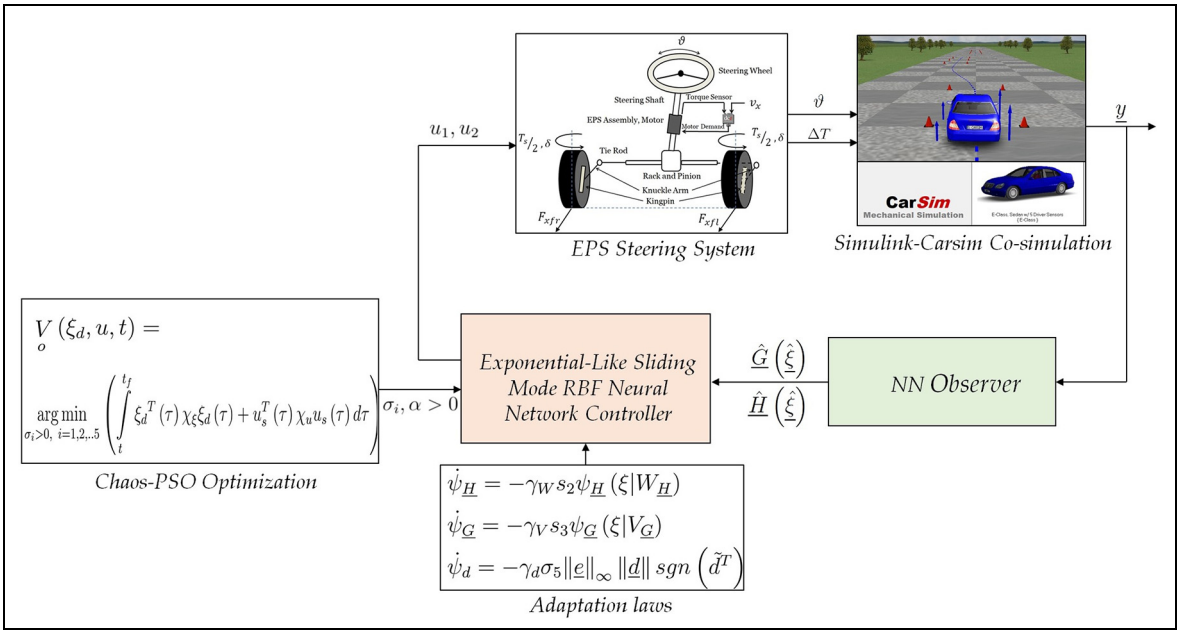

Figure 3. Block diagram of the proposed control algorithm.

presumed that within the defined compact region, the approximation errors are:

$$|\varepsilon(\xi)| \leqslant \Xi \qquad \forall\, \Xi \in R \tag{32}$$

where $\Xi \geqslant 0$ represents the unknown upper-limit which is also the least nonnegative factor in order to meet the inequality described in (32).

Controller design

On the basis of the arguments explored, the developed control system will hold the capacity to approximate the unknown system dynamics by estimating the unknown functions $\underline{H}(\xi, \dot{\xi}, \ldots, \xi^{(n-1)})$ and $\underline{G}(\xi, \dot{\xi}, \ldots, \xi^{(n-1)})$. Once the system dynamics is appropriately approximated, the modified sliding surface is introduced to ensure the closed-loop system stability by employing the Lyapunov theory. Accordingly, the approximated functions related to $\underline{H}(\xi, \dot{\xi}, \ldots, \xi^{(n-1)})$ and $\underline{G}(\xi, \dot{\xi}, \ldots, \xi^{(n-1)})$ are expressed through the weight vectors as:

$$\begin{aligned} \widehat{\underline{H}}(\xi|W_{\underline{H}}) &= W_{\underline{H}}^T \psi_{\underline{H}}(\xi) + \varepsilon_1 \\ \widehat{\underline{G}}(\xi|V_{\underline{G}}) &= V_{\underline{G}}^T \psi_{\underline{G}}(\xi) + \varepsilon_2 \end{aligned} \tag{33}$$

Theorem 1. Asymptotic stability of the system shown in (13) is accomplished in light of the adaptation laws as follows:

$$\begin{aligned} \dot{\psi}_{\underline{H}} &= -\gamma_W s_2 \psi_{\underline{H}}(\xi|W_{\underline{H}}) \\ \dot{\psi}_{\underline{G}} &= -\gamma_V s_3 \psi_{\underline{G}}(\xi|V_{\underline{G}}) \\ \dot{\psi}_d &= -\gamma_d \sigma_5 \|\underline{e}\|_\infty \|\underline{d}\| sgn(\tilde{d}^T) \end{aligned} \tag{34}$$

where γ_d, γ_W, and γ_V denote the learning speed of the associated functions. Moreover, σ_5 is employed as a control design coefficient, s_2 and s_3 serve as sliding surfaces and the disturbances magnitude is constrained by $\overline{d}$.

Proof. One can consider the approximation errors of the system functions with $\tilde{W}_{\underline{H}}^T$, $\tilde{V}_{\underline{H}}^T$ and $\tilde{d} = d - \hat{d}(\psi_d)$. The estimated disturbance function and the adaptation parameter are shown by $\hat{d}(\psi_d)$ *and* ψ_d, respectively. Additionally, the following sliding variables are chosen:

$$\begin{aligned} s_1 &= \dot{\underline{e}} + \lambda \underline{e} \\ s_2 &= \int_0^t \tilde{W}_{\underline{H}}^T \psi_{\underline{H}}(\xi) + \varepsilon_1 d\tau \\ s_3 &= \int_0^t \tilde{V}_{\underline{G}}^T \psi_{\underline{G}}(\xi) + \varepsilon_2 d\tau \end{aligned} \tag{35}$$

where λ denotes an arbitrary positive design coefficient. Moreover, it is known that the common reaching rules developed for the sliding surface decreases the control stability and brings about the undesired chattering issue.[5] Furthermore, a buffeting switch region exists around the equilibrium and thus, a modified reaching law is practiced as follows[5]:

$$\begin{aligned} \dot{s}_1 = &-\sigma_1 \|e\|_\infty \exp(-\sigma_2 |s_1|) sgn(s_1) \\ &- \frac{\sigma_3 \|e\|_\infty s_1}{\sigma_4 \exp(-\sigma_1 |s_1|) + \sigma_5} \end{aligned} \tag{36}$$

where $\sigma_i \;\; i = 1, 2, 3, 4$, serve as control design coefficients. Additionally, $\|e\|_\infty$ represents the norm of tracking error vector under the condition of $\lim_{t \to \infty} \|e\|_\infty = 0$. The Lyaunov function is defined as:

$$V(t) = \frac{1}{2}\sum_{i=1}^{3} s_i{}^2 + \frac{1}{2\gamma_W}\tilde{W}_{\underline{H}}\tilde{W}_{\underline{H}}^T + \frac{1}{2\gamma_V}\tilde{V}_{\underline{G}}\tilde{V}_{\underline{G}}^T + \frac{1}{2\gamma_D}\tilde{D}\tilde{D}^T \tag{37}$$

Differentiation of (37) results in:

$$\dot{V}(t) = \sum_{i=1}^{3} s_i\dot{s}_i - \frac{1}{\gamma_W}\tilde{W}_{\underline{H}}^T\dot{\hat{W}}_{\underline{H}} - \frac{1}{\gamma_V}\tilde{V}_{\underline{G}}^T\dot{\hat{V}}_{\underline{G}} - \frac{1}{\gamma_D}\tilde{d}^T\dot{\hat{d}} \tag{38}$$

Accordingly, (38) can be written as:

$$\begin{aligned}\dot{V}(t) = &-\sigma_1\|e\|_\infty \exp(-\sigma_2|s_1|)|s_1| \\ &-s_1{}^2\frac{\sigma_3\|e\|_\infty}{\sigma_4\exp(-\sigma_1|s_1|)+\sigma_5} + \left(\tilde{W}_H^T\psi_H(\xi)+\varepsilon_1\right)s_2 \\ &+ \left(\tilde{V}_G^T\psi_G(\xi)+\varepsilon_2\right)s_3 - \frac{1}{\gamma_W}\dot{\hat{W}}\tilde{W}^T - \frac{1}{\gamma_V}\dot{\hat{V}}\tilde{V}^T\end{aligned} \tag{39}$$

In light of the fact that the estimation errors of $\varepsilon_1(\xi)$ and $\varepsilon_2(\xi)$ are upper-constrained values, one can simply deduce that $\varepsilon_1(\xi)s_2 + \varepsilon_2(\xi)s_3 \ll \eta$ where η is a properly strict non-negative constant. Incorporating $\eta \leqslant \xi_5\|e\|_\infty\|\tilde{d}^T\bar{d}\|$ in (40) results in:

$$\begin{aligned}\dot{V}(t) = &-\sigma_1\|e\|_\infty \exp(-\sigma_2|s_1|)|s_1| \\ &-s_1{}^2\frac{\sigma_3\|e\|_\infty}{\sigma_4\exp(-\sigma_1|s_1|)+\sigma_5} + \\ &\left(\tilde{W}_H^T\psi_H(\xi)+\varepsilon_1\right)s_2 + \left(\tilde{V}_G^T\psi_G(\xi)+\varepsilon_2\right)s_3 \\ &-\eta - \frac{1}{\gamma_W}\tilde{W}_{\underline{H}}{}^T\dot{\hat{W}}_{\underline{H}}{}^T - \frac{1}{\gamma_V}\tilde{V}_{\underline{G}}{}^T\dot{\hat{V}}_{\underline{G}}{}^T - \frac{1}{\gamma_D}\dot{\tilde{d}}\tilde{d}^T \\ &+ \sigma_5\|e\|_\infty\tilde{d}^T\|\bar{d}\|sgn(\tilde{d}^T)\end{aligned} \tag{40}$$

$$\begin{aligned}\dot{V}(t) = &-\sigma_1\|e\|_\infty\exp(-\sigma_2|s_1|)|s_1| \\ &-s_1^2\frac{\sigma_3\|e\|_\infty}{\sigma_4\exp(-\sigma_1|s_1|)+\sigma_5} + (\tilde{W}_H^T\psi_H(\xi)+\varepsilon_1)s_2 + \\ &(\tilde{V}_G^T\psi_G(\xi)+\varepsilon_2)s_3 - \eta - \frac{1}{\gamma_W}\tilde{W}_{\underline{H}}^T\dot{\psi}_{\underline{H}} - \frac{1}{\gamma_V}\tilde{V}_{\underline{G}}^T\dot{\psi}_{\underline{G}} \\ &-\frac{1}{\gamma_D}\dot{\psi}_{\underline{d}}\tilde{d}^T + \sigma_5\|e\|_\infty\tilde{d}^T\|\bar{d}\|sgn(\tilde{d}^T)\end{aligned} \tag{41}$$

Equation (41) results in (42) by plugging-in the terms in (34):

$$\begin{aligned}\dot{V}(t) = &-\sigma_1\|e\|_\infty\exp(-\sigma_2|s_1|)|s_1| \\ &-s_1{}^2\frac{\sigma_3\|e\|_\infty}{\sigma_4\exp(-\sigma_1|s_1|)+\sigma_5} - \eta < 0\end{aligned} \tag{42}$$

wherein, the proposed control system is globally asymptotically stable. Furthermore, the convergence of the tracking error e to zero in finite time is accomplished, which finalizes the proof.

Search of optimality

An important aspect of designing the adaptive robust controllers is to identify appropriate constants for the derived adaptation laws.

In addition to the global asymptotic stability, the rapid convergence and constraints on the control inputs are other issues that many of robust adaptive control studies simply exclude in the design of control analysis. To this end, the following cost-function is designed to be minimized according to the saturated control inputs and the tracking error minimization of ξ_d, and χ_ξ and χ_u are positive definite and positive semi-definite weighting matrices with appropriate dimensions according to (43):

$$\underset{o}{V}(\xi_d, u, t) = \underset{\sigma_i>0,\ i=1,2,..5}{\arg\min} \left(\int_t^{t_f} \xi_d{}^T(\tau)\chi_\xi\xi_d(\tau) + u_s^T(\tau)\chi_u u_s(\tau)d\tau\right) \tag{43}$$

subject to the dynamics in (1) and (44):

$$\begin{aligned}&u_s = sat(u) = sgn(u).\min\{u, u_{\max}\} \\ &\xi_d{}^T(t)\chi_d x(t) > 0; u_s{}^T(t)\chi_u u_s(t) \geqslant 0,\ \forall t \geqslant 0, \\ &\sigma_i, \alpha > 0 \quad i = 1, 2, ...5\end{aligned} \tag{44}$$

The above optimization problem is solved through a modified Particle swarm optimization (PSO) approach. PSO is commonly known as the most popular metaheuristic optimization tool employed in diverse optimization problems.[27,28] Nevertheless, the premature convergence in multimodal problems serves as a main concern for this approach.[27] A fine tuning of the PSO parameters, such as the inertial parameters, improves the performance only slightly but at the exchange of a huge computational load. In classical PSO algorithms, the particles possess the problem space and embark on searching through stochastically zigzag-like orientations.[27] This pattern is indispensable to constantly move toward the global and local bests at once (i.e. $\tilde{x}g_i$, and $\tilde{x}p_i$) and to promise the steady convergence to the global optimum result. For the brevity, the interested reader may refer to our previous paper on this optimization method.[28]

Results and discussion

The model employed in this study for the dynamics of the vehicle is a commonly practiced approach among the reported studies (e.g. Taghavifar et al.[13]). However, the present study contains the hugely influential dynamics of the steering system and adds the effect to the steering mechanism constrains into consideration. In addition to the nonlinearities introduced due to the steering system structure, the tire model nonlinearity accounts for the range after tire force saturation. The effectiveness of the proposed controller is investigated across various steering inputs. Additionally, the

obtained responses for the vehicle are compared to the open-loop system to assess the benefits of employing the employed control system. The effectiveness of the proposed controller is also validated against the recently employed techniques for the vehicle lateral stabilization. The maneuvers employed for this purpose involved (i) a rectangular pulse, (ii) a step steering input, and (iii) a double-lane change to account for the entire steady-state and transient conditions. Furthermore, simulations are carried out for a vehicle at a relatively high speed of 100 km/h on a road characterized with a relatively low-adhesion coefficient of 0.4. Further simulation parameters are presented in Table 1.

Table 1. Vehicle parameters used for simulation.

Parameter (unit)	Value
m (kg)	1480
I_z (kgm^2)	2350
I_s (kgm^2)	4200
l_f (m)	1.05
l_r (m)	1.63
$\hat{C}_f$ (N/rad)	67,500
$\hat{C}_r$ (N/rad)	74,500
C_s (Nms/rad)	225
K_s (Nm/rad)	10,000

Rectangular pulse

Figure 4 demonstrates a comparison of the yaw-rate, slip-angle, and the steering wheel angles of the vehicle due to the proposed controller and an optimal robust control method reported in the recent literature by the author of the present paper.[13] Although both the vehicles with the employed controllers demonstrate the capacities to follow the desired yaw-rate signal, the vehicle with the proposed controller can converge much faster and closer to the desired yaw-rate. Additionally, the slip-angle and yaw-rate states of the vehicle demonstrate quicker convergence and responsiveness as compared to the optimal robust controller. It is also evident that the proposed controller holds the capacity to suppress the slip-angle state of the vehicle in a more drastic manner (Figure 4). Not only the optimal robust controller lags to reach the desired yaw-rate value, it also demands more than 2 s to return to the steady condition compared to the proposed controller. Furthermore, the time histories of the steering-wheel angle are suggestive of an inadequate rotation to generate the vehicle turning during the maneuver.

Figure 5 illustrates the variations of the control inputs in terms of a combined AFS + DYC but in an individual manner. It is evident that the control signals are responsive and rapidly rise to catch up with the desired performance. A major concern in previous efforts of the combined AFS + DYC was the potential overload of one signal to take on the insufficient contributions from the other input. However, the range of variations for DYC stays within a reasonable band (i.e. maximum of 250 N.m.) due to the effective contribution of the AFS. It is also interesting to note that the vehicle efforts to generate the desired yaw-rate first by the aid of the AFS and the insufficiency are immediately compensated through the DYC input. Additionally, it is observed that AFS and DYC vary with a notable harmony that collectively contribute to address the desired maneuvering performance. The evident overshoot related to the yaw-rate response of the proposed method can be related to the quick rise time requirement. In terms of the output response, one can compromise between the rise time and the overshoot through the variations of the equivalent damping. The yaw-damping can be obtained through the tire construction and effective cornering stiffness.

Steady-state driving

In this section, a regularly tested steady-state test is considered according to the ISO 4138:2012 that describes the steady-state circular driving behavior through the open-loop test methods.[29] The desired yaw-rate to perform such a test is illustrated in Figure 6. Additionally, the yaw-rate responses of the car by employing the optimal robust controller and the proposed controller are compared in Figure 6, to verify the effectiveness of the developed algorithm. The considerably rapid rise time and setting time for the proposed controller compared to the benchmarking algorithm further confirms the capacity of the developed method for stabilization and to reach the desired trajectory. Additionally, the yaw-rate response for the optimal robust controller generates a little oscillatory characteristic which is obviously an undesirable behavior and promotes discomfort and instability for the passenger. Although there is a small overshoot for the proposed method, the rapider stabilization for about 2 s before the optimal robust algorithm is desirable for a safer maneuvering capacity of the vehicle. One should also note that such a time lag at 100 km/h can be bring about non-compensable perils and lack of vehicle lateral stability. Figure 6 also illustrates the time-histories of the vehicle slip-angle, which also confirms the rapid responsiveness of the proposed method which contributes to maximize the lateral acceleration about the corner. The steering wheel angle state comparison between the proposed controller and the optimal robust algorithm also demonstrates that a larger steering wheel angle is imposed on the vehicle with the developed technique. Of course, a small steering angle to maintain stability of the vehicle is desirable by substantially reducing the steering effort demand from the driver.

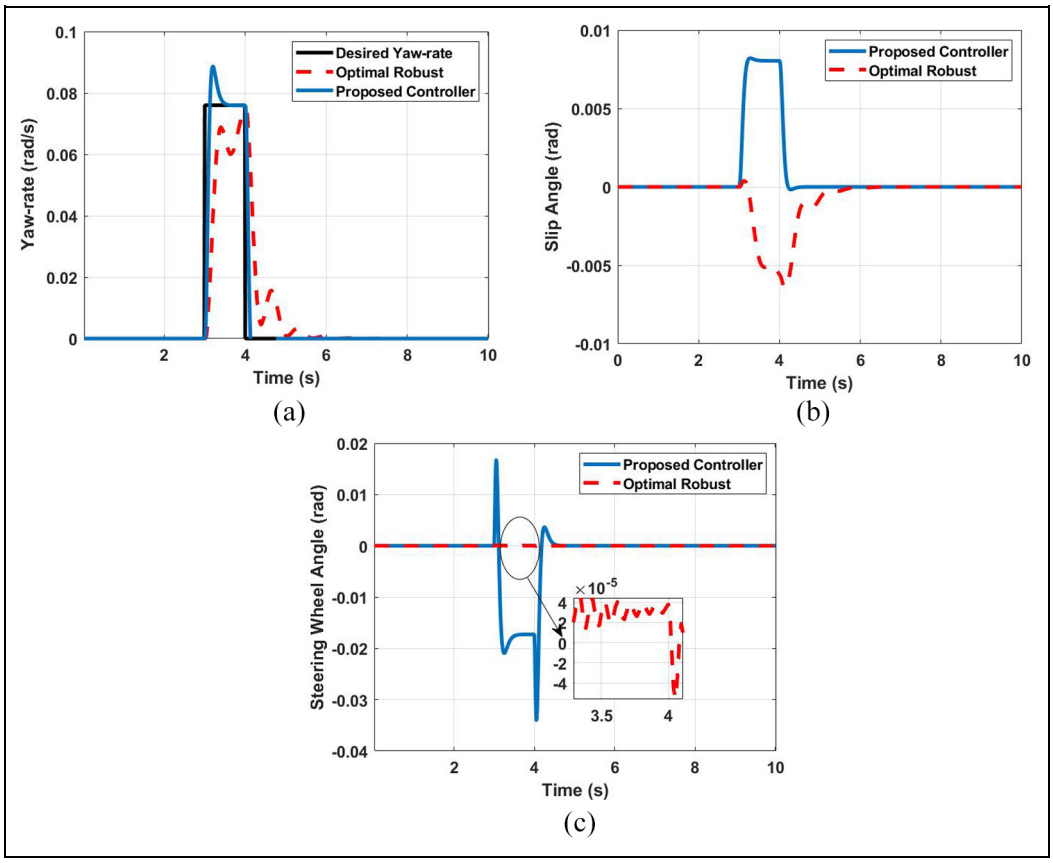

Figure 4. Time-histories of vehicle: (a) yaw-rate, (b) slip-angle, and (c) steering-wheel angle during rectangular pulse input.

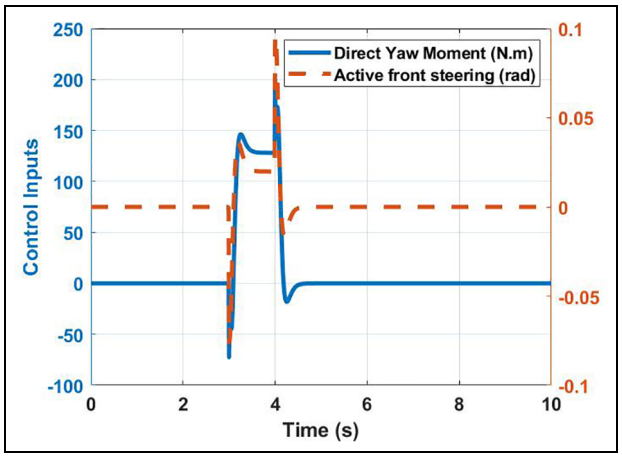

Figure 5. Time-histories of vehicle control inputs during rectangular pulse input.

Double-lane change

The final testing platform in this paper for the effectiveness of the proposed controller is to perform a transient-based DLC maneuver according to ISO 3888-1:2018. It is appreciated from Figure 7 that not only the yaw-rate is bounded at lower range for the vehicle with optimal robust controller, but there is a considerable phase lag as compared to the desired-yaw rate. However, the rapid response of the proposed controller to the yaw-rate change is suggestive of its effectiveness to ensure the vehicle lateral stability. Additionally, the sip-angle and steering-wheel angle responses of the vehicle with the optimal robust controller are compared to the proposed controller in Figure 7. It is evident that there exists an observable difference between their tendencies. Finally, Figure 7 illustrates the variations of the tracking error for the yaw-rate actual following the desired yaw-rate. It is noticed that the largest variations belong to the optimal robust control method and the proposed algorithm approves efficient to constrain such tracking errors. Additionally, Figure 8 demonstrates the lateral force components applied to the front and rear wheels. It is evident that the generalized lateral forces are maintained in reasonable regions. This guarantees the existence of the directional acceleration and thus, nonzero lateral speed of the vehicle during this transient maneuver. A certain level of the lateral speed contributes to a smooth cornering experience. Additionally, Figure 8 illustrates the directional acceleration variations for the vehicle under the proposed control framework. There are slight variations of the longitudinal acceleration that are imposed through the DYC approach. The largest variations are observed for the lateral acceleration and the drastic changes might be attributed to the sudden path changes and the demand to generate the yaw-rate owing to the nonholonomic constraints existing for the vehicle. Figure 9

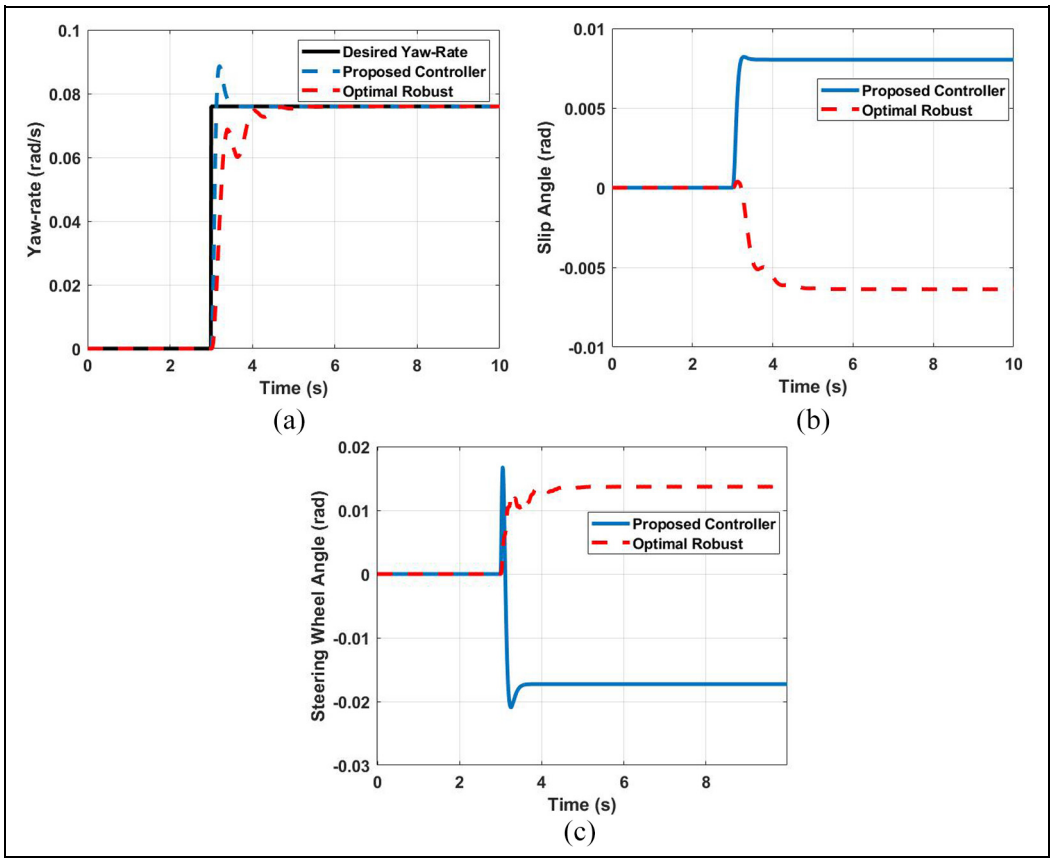

Figure 6. Time-histories of vehicle: (a) yaw-rate, (b) slip-angle, and (c) steering-wheel angle during CRC maneuver.

represents the path tracking performance of the vehicle with the optimal robust and the proposed controller in the global coordinate system. It is appreciated that the DLC maneuverer is carried out perfectly, with only infinitesimal tracking error, unlike the optimal robust counterpart which brings about a considerable offset level together with a large phase lag. It is also further confirmed that the proposed controller effective and robust even though a satisfactory path following is accomplished with fluctuations in the longitudinal acceleration.

Robustness to external disturbances

The robustness of a controller to structured and unstructured uncertainties plays a significant role in the overall performance of the vehicle. Therefore, a gust of cross-wind effect was investigated on the robustness of the proposed controller, compared to the optimal robust and the system without any controller. The obtained results are plotted in the global-coordinate system to view the trajectory of the vehicle while intending to travel on a straight path subject to the gust of wind for duration of 1 s in the shape of a rectangular pulse with the magnitude of 2000 N. It is known that the trajectory of a vehicle in a neutral-steering (NS) manner is more desirable that the under-steering (US), while over-steering (OS) promotes instability. The obtained results demonstrate that the proposed controller is not affected by the cross-wind gust during its travel while the optimal robust has demonstrated a US characteristic and has shifted more than 2 m laterally in less than 300 m of the longitudinal travel (Figure 10). However, the weakest performance is attributed to the vehicle without any controller than exhibits a largely OS performance and vehicle stability is lost in less than 100 m. Therefore, the inevitable demand for a high-performance controller as proposed in this paper is encapsulated in light of the represented results in Figure 10.

Conclusions

The present paper mainly contributes through the development and synthesis of a coordinated AFS + DYC control framework in order to enhance the vehicle lateral stability and maneuverability. For this purpose, the steering mechanism dynamics and states are also incorporated. The approximation capacity of the radial basis function (RBF) neural network system is also employed for the closed-loop system as well as the designed state observer. The adaptation mechanism is obtained through the Lyapunov stability theory. In order to improve the robustness of the closed-loop vehicle, the SMC approach is practiced while the sliding surface of the tracking errors

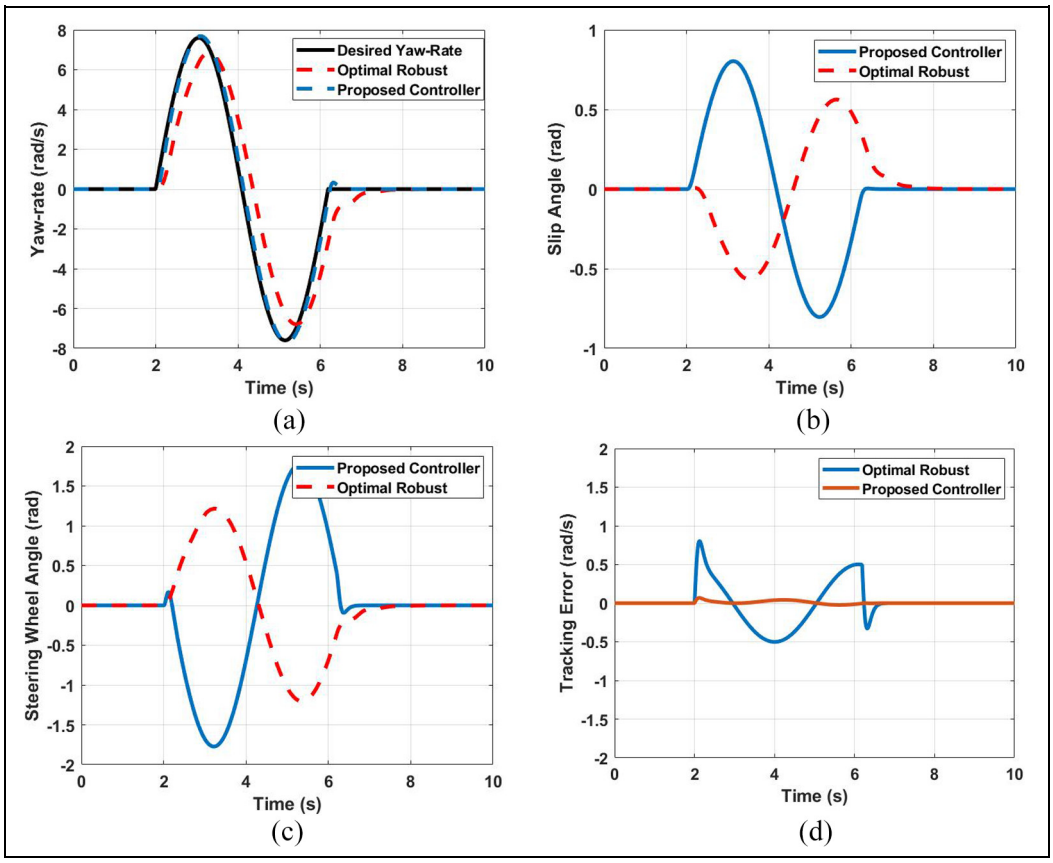

Figure 7. Time-histories of vehicle: (a) yaw-rate, (b) slip-angle, (c) steering-wheel angle, and (d) yaw-tracking error during DLC maneuver.

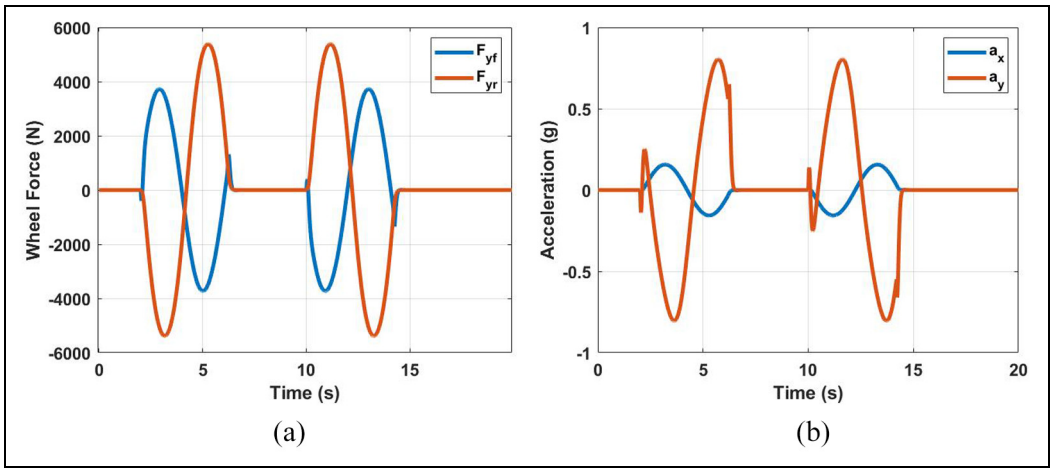

Figure 8. Time-histories for: (a) front and rear wheels lateral forces and (b) directional accelerations of vehicle C.G. during DLC maneuver.

converges to the asymptotic stability condition through the design of a smooth exponential reaching law. The effectiveness of the proposed control scheme was evaluated against a high-performance optimal robust control technique as well as the open-loop system. In order to assess the robustness of the proposed algorithm, the structured and unstructured uncertainties were also incorporated in terms of the parametric uncertainties such as the tire cornering stiffness and cross-wind gust disturbance. In order to analyze the closed-loop system against the extraneous disturbances, it was traveled on a straight path subject to the gust of wind for duration of 1 s in the shape of a rectangular pulse with the magnitude of 2000 N. The obtained results demonstrate that the proposed controller is not affected by the cross-wind gust during its travel while the optimal

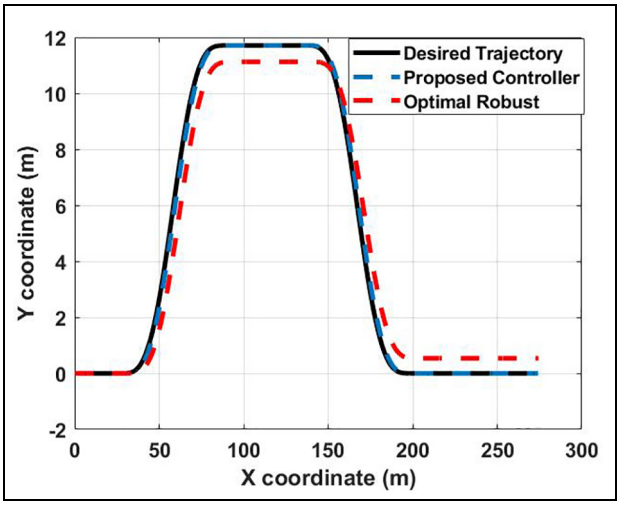

Figure 9. Global trajectory of the vehicle for path following during DLC maneuver.

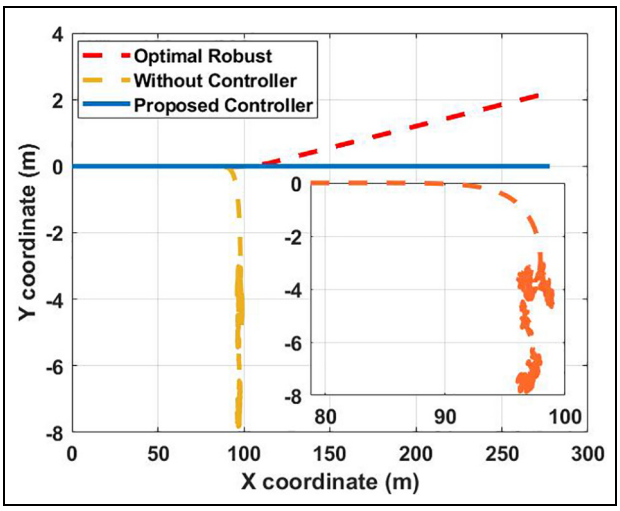

Figure 10. Global trajectory representation of vehicle subject to cross-wind disturbance under different control schemas.

robust has demonstrated a US characteristic and has shifted more than 2 m laterally in less than 300 m of the longitudinal travel. However, the weakest performance is attributed to the vehicle without any controller than exhibits a largely OS performance and vehicle stability is lost in less than 100 m.

Declaration of conflicting interests

The author declared no potential conflicts of interest with respect to the research, authorship, and/or publication of this article.

Funding

The author received no financial support for the research, authorship, and/or publication of this article.

ORCID iD

Hamid Taghavifar https://orcid.org/0000-0002-2407-8393

References

1. Hu C, Wang Z, Taghavifar H, et al. MME-EKF-based path-tracking control of autonomous vehicles considering input saturation. *IEEE Trans Veh Technol* 2019; 68(6): 5246–5259.
2. Taghavifar H. Neural network autoregressive with exogenous input assisted multi-constraint nonlinear predictive control of autonomous vehicles. *IEEE Trans Veh Technol* 2019; 68(7): 6293–6304.
3. Wei C, Romano R, Merat N, et al. Risk-based autonomous vehicle motion control with considering human driver's behaviour. *Transp Res Part A Policy Pract* 2019; 107: 1–14.
4. Guo H, Liu F, Xu F, et al. Nonlinear model predictive lateral stability control of active chassis for intelligent vehicles and its FPGA implementation. *IEEE Trans Syst Man Cybern Syst* 2017; 49(1): 2–13.
5. Taghavifar H and Rakheja S. Path-tracking of autonomous vehicles using a novel adaptive robust exponential-like-sliding-mode fuzzy type-2 neural network controller. *Mech Syst Signal Process* 2019; 130: 41–55.
6. Mohammadzadeh A and Taghavifar H. A robust fuzzy control approach for path-following control of autonomous vehicles. *Soft Comput* 2020; 24(5): 3223–3235.
7. Sun W, Zhang J and Liu Z. Two-time-scale redesign for antilock braking systems of ground vehicles. *IEEE Trans Ind Electron* 2018; 66(6): 4577–4586.
8. Wang R, Hu C, Yan F, et al. Composite nonlinear feedback control for path following of four-wheel independently actuated autonomous ground vehicles. *IEEE Trans Intell Transp Syst* 2016; 17(7): 2063–2074.
9. Hu C, Gao H, Guo J, et al. Rise-based integrated motion control of autonomous ground vehicles with asymptotic prescribed performance. *IEEE Trans Syst Man Cybern Syst*. Epub ahead of print 2020. DOI: 10.1109/tsmc.2019.2950468.
10. Hu C, Wang R, Yan F, et al. Robust composite nonlinear feedback path-following control for independently actuated autonomous vehicles with differential steering. *IEEE Trans Transp Electrif* 2016; 2(3): 312–321.
11. Cui Q, Ding R, Wei C, et al. A hierarchical framework of emergency collision avoidance amid surrounding vehicles in highway driving. *Control Eng Pract* 2021; 109: 104751.
12. Zhang H and Wang J. Vehicle lateral dynamics control through AFS/DYC and robust gain-scheduling approach. *IEEE Trans Veh Technol* 2015; 65(1): 489–494.
13. Taghavifar H, Hu C, Taghavifar L, et al. Optimal robust control of vehicle lateral stability using damped least-square backpropagation training of neural networks. *Neurocomputing* 2020; 384: 256–267.
14. Mohammadzadeh A and Taghavifar H. A novel adaptive control approach for path tracking control of autonomous vehicles subject to uncertain dynamics. *Proc IMechE, Part D: J Automobile Engineering* 234(8): 2115–2126.
15. Taghavifar H, Hu C, Qin Y, et al. EKF-neural network observer based type-2 fuzzy control of autonomous

vehicles. *IEEE Trans Intell Transp Syst*. Epub ahead of print 2020. DOI: 10.1109/tits.2020.2985124.
16. Li B, Rakheja S and Feng Y. Enhancement of vehicle stability through integration of direct yaw moment and active rear steering. *Proc IMechE, Part D: J Automobile Engineering* 2016; 230(6): 830–840.
17. Guo J, Luo Y, Li K, et al. Coordinated path-following and direct yaw-moment control of autonomous electric vehicles with sideslip angle estimation. *Mech Syst Sig Process* 2018; 105: 183–199.
18. Zhao W, Zhang H and Li Y. Displacement and force coupling control design for automotive active front steering system. *Mech Syst Sig Process* 2018; 106: 76–93.
19. Guo J, Wang J, Luo Y, et al. Robust lateral control of autonomous four-wheel independent drive electric vehicles considering the roll effects and actuator faults. *Mech Syst Sig Process* 2020; 143: 106773.
20. Hu C, Jing H, Wang R, et al. Robust H∞ output-feedback control for path following of autonomous ground vehicles. *Mech Syst Sig Process* 2016; 70: 414–427.
21. Jing H, Wang R, Wang J, et al. Robust H∞ dynamic output-feedback control for four-wheel independently actuated electric ground vehicles through integrated AFS/DYC. *J Franklin Inst* 2018; 355(18): 9321–9350.
22. Jin X, Yu Z, Yin G, et al. Improving vehicle handling stability based on combined AFS and DYC system via robust Takagi-Sugeno fuzzy control. *IEEE Trans Intell Transp Syst* 2017; 19(8): 2696–2707.
23. Park M, Lee S, Kim M, et al. Integrated differential braking and electric power steering control for advanced lane-change assist systems. *Proc IMechE, Part D: J Automobile Engineering* 2015; 229(7): 924–943.
24. Zhang J and Li J. Integrated vehicle chassis control for active front steering and direct yaw moment control based on hierarchical structure. *Trans Inst Meas Control* 2019; 41(9): 2428–2440.
25. Aripin M, Md Sam Y, Danapalasingam KA, et al. A review of active yaw control system for vehicle handling and stability enhancement. *Int J Veh Technol* 2014; 2014: 1–15.
26. Taghavifar H. Reduced vibration of off-road vehicle nonlinear suspension system using an adaptive integral sliding mode-neural network controller. *Int J Dyn Control* 2020; 8(1): 291–301.
27. Gandomi AH, Yun GJ, Yang X-S, et al. Chaos-enhanced accelerated particle swarm optimization. *Commun Nonlinear Sci Numer Simul* 2013; 18(2): 327–340.
28. Taghavifar H and Rakheja S. Multi-objective optimal robust seat suspension control of off-road vehicles in the presence of disturbance and parametric uncertainty using metaheuristics. *IEEE Trans Intell Veh* 2019; 5(3): 372–384.
29. I. S. O. 4138:2002. Passenger cars–steady-state circular driving behavior–open-loop test methods. International Organization for Standardization, 2012.

Appendix

Notation

β	body slip
$\Delta C_{f,r}$	tire stiffness uncertainty
γ	yaw-rate
φ	heading angle
ϑ	steering wheel angle
C_s	steering damping
$F_{yf,r}$	tire lateral force
I_s	steering inertia moment
I_z	inertia moment
K_s	steering stiffness
l_b	track width
l_f, r	wheelbase components
m	mass
v_y	lateral speed
v_y	longitudinal speed
δ_f	wheel angle
ΔT	yaw moment
σ_c	castor trail
σ_n	pnemumatic trail
$\widetilde{C}_f$	nominal cornering stiffness
$C_{f,r}$	tire cornering stiffness
T_s	kingpin moment